STRUCTURAL BIOLOGY COMMUNICATIONS

ISSN 2053-230X

1.45 Å resolution structure of SRPN18 from the malaria vector *Anopheles gambiae*

David A. Meekins,[a] Xin Zhang,[a] Kevin P. Battaile,[b] Scott Lovell[c] and Kristin Michel[a]*

[a]Division of Biology, Kansas State University, USA, [b]IMCA–CAT, Hauptman–Woodward Medical Research Institute, Argonne National Laboratory, USA, and [c]Protein Structure Laboratory, Del Shankel Structural Biology Center, University of Kansas, USA. *Correspondence e-mail: kmichel@ksu.edu

Received 16 September 2016
Accepted 8 November 2016

Edited by T. C. Terwilliger, Los Alamos National Laboratory, USA

Keywords: serpins; serine proteases; insect immunity; enzyme inhibitors; mosquito; *Anopheles gambiae*; malaria vector.

PDB reference: SRPN18 from *Anopheles gambiae*, 5c98

Supporting information: this article has supporting information at journals.iucr.org/f

Serine protease inhibitors (serpins) in insects function within development, wound healing and immunity. The genome of the African malaria vector, *Anopheles gambiae*, encodes 23 distinct serpin proteins, several of which are implicated in disease-relevant physiological responses. *A. gambiae* serpin 18 (SRPN18) was previously categorized as non-inhibitory based on the sequence of its reactive-center loop (RCL), a region responsible for targeting and initiating protease inhibition. The crystal structure of *A. gambiae* SRPN18 was determined to a resolution of 1.45 Å, including nearly the entire RCL in one of the two molecules in the asymmetric unit. The structure reveals that the SRPN18 RCL is extremely short and constricted, a feature associated with noncanonical inhibitors or non-inhibitory serpin superfamily members. Furthermore, the SRPN18 RCL does not contain a suitable protease target site and contains a large number of prolines. The SRPN18 structure therefore reveals a unique RCL architecture among the highly conserved serpin fold.

1. Introduction

Serpins (serine protease inhibitors) represent the largest family of protease inhibitors and are found in all higher eukaryotes and some bacteria, archaea and viruses (Olson & Gettins, 2011; Silverman *et al.*, 2010). Proteolytic events are integral to a wide variety of signaling pathways and govern diverse physiological functions, such as development (Hashimoto *et al.*, 2003; Ligoxygakis *et al.*, 2003; Francis *et al.*, 2012), coagulation (Huntington, 2013), cell migration (Ravenhill *et al.*, 2010; Declerck & Gils, 2013; Yamamoto *et al.*, 2013; Huasong *et al.*, 2015), tumor suppression (Mahajan *et al.*, 2013), fibrinolysis (Rau *et al.*, 2007; Al-Horani, 2014) and immunity (Ashton-Rickardt, 2013; Silverman *et al.*, 2010; Gatto *et al.*, 2013). In general, the proteases that comprise these signaling pathways are expressed as zymogens, becoming activated upon proteolytic cleavage in order to elicit a rapid, controlled physiological response. Serpins function to silence these responses in order to avoid negative physiological consequences stemming from uncontrolled activation (Olson & Gettins, 2011). Recent studies in insects have implicated serpins in a variety of essential physiological events, including development, mating, anticoagulation and immunity (Silverman *et al.*, 2010; Gubb *et al.*, 2010; Meekins *et al.*, 2016).

Serpins typically range in size from 350 to 400 residues and contain a highly conserved fold consisting of three β-sheets (A, B and C) surrounded by up to nine α-helices (A–I) (Huntington, 2011). The central motif governing serpin

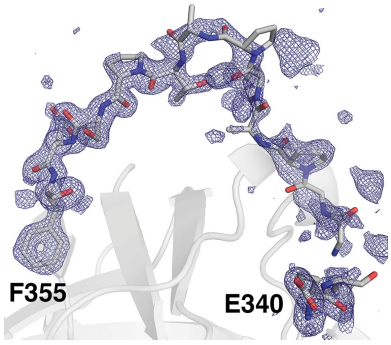

activity is the reactive-center loop (RCL), a solvent-exposed loop that acts as a bait for the target protease. Despite the conservation of the overall serpin fold, there is a high degree of diversity among the RCLs of different serpins (Irving *et al.*, 2000). The specificity and regulation of serpin–protease interactions largely stems from the primary sequence and conformation of the RCL (Irving *et al.*, 2000; Ye *et al.*, 2001). An essential component of the RCL is the scissile bond, which is defined as the peptide bond between two amino-acid residues denoted P1 and P1′ and cleaved by the target protease, forming an acyl-enzyme intermediate (Loebermann *et al.*, 1984). After formation of the intermediate complex, the serpin undergoes a dramatic conformational transformation whereby the RCL inserts into β-sheet A, forming an additional β-strand, and the protease is translocated to the opposing end of the serpin (Stratikos & Gettins, 1999; Huntington, McCoy *et al.*, 2000; Dunstone & Whisstock, 2011). The biophysical basis of this inhibitory transformation stems from the higher stability of the resultant complex compared with the native, metastable structure of the serpin (Whisstock & Bottomley, 2006; Huntington, 2006). As a result of the conformational change, both the serpin and protease are unable to perform further reactions and remain in an SDS-stable complex until degraded by cellular processes (Huntington, Read *et al.*, 2000). Thus, the canonical serpin mechanism for inactivating proteases is designated suicide inhibition.

Interestingly, many serpins do not function as protease inhibitors *via* the canonical inhibitory mechanism despite containing the conserved serpin fold (Stein *et al.*, 1989). Although many of the non-inhibitory serpins are susceptible to proteolytic cleavage, they invariably contain structural alterations, mostly within the RCL, that are unfavorable for rapid formation of the inhibitory complex. These features include α-helical secondary structure in the RCL, bulky residues in the RCL hinge region, a highly constrained RCL, complete hydrogen bonding in the breach region of β-sheet A, proline residues preceding the scissile bond or the presence of a glycosylation site within the RCL (Hopkins *et al.*, 1993; Huntington *et al.*, 1997; Simonovic *et al.*, 2001; Al-Ayyoubi *et al.*, 2004; Chaillan-Huntington *et al.*, 1997; Widmer *et al.*, 2012; Stein *et al.*, 1991; Hood *et al.*, 1994; McCarthy & Worrall, 1997). These non-inhibitory serpins invariably contain distinct structural features associated with protein or ligand binding that form the basis of their physiological function (Simonovic *et al.*, 2001; Al-Ayyoubi *et al.*, 2004; Widmer *et al.*, 2012; Zhou *et al.*, 2006; McGowan *et al.*, 2006; Klieber *et al.*, 2007). In addition, several serpins have been discovered that inhibit cysteine proteases *via* a noncanonical mechanism whereby the protease becomes trapped in a complex with the RCL until both the protease and the serpin are degraded by proteolytic processes (Guo *et al.*, 2015; Fish & Bjork, 1979; Mast *et al.*, 1992; Zhou *et al.*, 1997; Annand *et al.*, 1999; Schick *et al.*, 1998). Despite their noncanonical properties, non-inhibitory and cysteine protease-inhibiting serpins are critical to a variety of essential biological processes.

Serpins in the African malaria vector mosquito *Anopheles gambiae* (designated SRPNs) have gained attention as key regulators of immunity and potential targets for vector control (Gulley *et al.*, 2013; Suwanchaichinda & Kanost, 2009). 18 *SRPN* genes encoding 23 proteins have been identified in *A. gambiae*, but only a limited number have been characterized (Gulley *et al.*, 2013; Christophides *et al.*, 2002, 2004). The only known targets of inhibitory serpins in *A. gambiae* are clip domain-containing serine proteases (CLIPs; An, Budd *et al.*, 2011). Catalytically active CLIPs circulate as zymogens, becoming active upon cleavage between the CLIP and serine protease (SP) domains, thus initiating a proteolytic cascade that culminates in a specific physiological response (Barillas-Mury, 2007). *A. gambiae* CLIPB9 has been shown to convert pro-phenoloxidase (PPO) to phenoloxidase (PO), which results in a melanization immune response (An, Budd *et al.*, 2011). SRPN2 inhibits CLIPB9 in *A. gambiae*, thus regulating melanization and avoiding the negative-fitness consequences of an uncontrolled immune response (An, Budd *et al.*, 2011; Michel *et al.*, 2005). Furthermore, SRPN6 and SRPN10 have been shown to be upregulated in response to parasite or bacterial infection, and SRPN6 has been shown to have antiparasitic effects (Danielli *et al.*, 2003; Abraham *et al.*, 2005). Despite these insights into the importance of mosquito serpins, our understanding of the protease–serpin networks that regulate mosquito physiology is in its infancy and information regarding the uncharacterized *A. gambiae* serpins is limited. Insights into these uncharacterized *A. gambiae* serpins is important to further understand the physiology and vector competence of this medically important mosquito species.

SRPN18 (AGAP007691; XP_003435746) is among the sparsely characterized serpins in *A. gambiae*. Previous studies indicate that *A. gambiae* SRPN18 is expressed throughout all life stages in multiple tissues and the hemolymph, and it is predicted to be secreted based on the presence of a signal peptide (Suwanchaichinda & Kanost, 2009). SRPN18 expression doubles within 3 h of a blood meal and returns to pre-blood-meal levels within 24 h post-blood feeding (Marinotti *et al.*, 2006). However, its role in *A. gambiae* physiology is entirely unknown. The *SRPN18* gene clusters tightly with *SRPN7* and *SRPN14* on chromosomal arm 2L, close to the *SRPN2* cluster (Suwanchaichinda & Kanost, 2009). Microarray data indicate that *AgSRPN18* is repressed upon infection with *Wolbachia* bacteria, which have been shown to protect mosquitoes from *Plasmodium* infection, although the significance of these data is unknown (Kambris *et al.*, 2010; Hughes *et al.*, 2011). Previous examination of the primary sequence of the SRPN18 RCL resulted in the prediction that SRPN18 is non-inhibitory (Gulley *et al.*, 2013; Suwanchaichinda & Kanost, 2009). This is based on the absence of an RCL hinge region, a conserved span of four residues that provides RCL flexibility and is integral for inhibitory complex formation.

Here, we present the structure of *A. gambiae* SRPN18 to a resolution of 1.45 Å. The high-resolution crystal structure of SRPN18 was determined, including nearly complete resolution of the RCL. These data provide additional insights into mosquito serpins and may provide a basis for identifying the physiological function of SRPN18 in *A. gambiae*.

Table 1
Macromolecule-production information.

Source organism	*A. gambiae*
DNA source	Adult female *A. gambiae* G3 strain
Forward primer	5′-TCATCACGGCGATCCTACGACAG-3′
Reverse primer	5′-TTGAATTCTCAAAACTGTTCATCGG-3′
Cloning vector	Not applicable
Expression vector	pET-28a
Expression host	*E. coli* BL21 (DE3)
Complete amino-acid sequence of the construct produced	MGHHHHHHGDPTTDDAIVAANNKFTLEYFKACYD-EKCNCAVSPYHVRLALSMFYPLAGAAVQEDFQ-VAFGLPEDVHAAIEQQQRLAQQLHDGQHLKAL-SFVLVEETLRLDSEFERLFHRTFQTTVEPVDL-TDDIPSALAVNSFYQRANTEIEDFIGEGDVFS-LPPCHKLMLFSGVSVLTPLAIRFNPADTALEL-FQFINAPTQRVSTMHTTAFVRRCLHNELRCKV-VDMPFDAASGLSMLVLLPYDGTELRQIVNSIT-PAHLAQIDERLQSCWTDLKLPKFFVREKTDPK-QTLGKLGYGGVFEIDDLHVFHDSGRTRLNGFI-QHCYLAVSESGSGIPAPPDTPSEFEFHANRPF-MFLIRRTMDGNVLQVGNFSKYIDPDEQF

2. Materials and methods

2.1. Macromolecule production

2.1.1. SRPN18 cloning and recombinant SRPN18 protein expression. cDNA fragments encoding full-length mature proteins were amplified using the gene-specific primers SRPN18-1F, 5′-TCATCACGGCGATCCTACGACAG-3′, and SRPN18-1R, 5′-TT**GAATTC**TCAAAACTGTTCATCGG-3′. The reverse primer contained an EcoRI restriction site (bold). A second round of PCR was performed with the forward primer SRPN18-2F containing codons for a His_6 tag (underlined) as well as an NcoI site (bold), 5′-AT**CCATGG**GCCAT-CATCATCATCATCATCACGGC-3′, with SRPN18-1R as the reverse primer. The PCR products were digested with NcoI and EcoRI, and then inserted into the pET-28a vector (Novagen) using the same restriction sites. The resulting plasmid (pET28a-SRPN18) was transformed into BL21 (DE3) competent *Escherichia coli* cells and stored at −80°C (Table 1).

Recombinant SRPN18 protein was produced using an *E. coli* expression system (Table 1). The full coding region, minus the predicted signal peptide, was amplified using gene-specific primers. SRPN18 protein was expressed using BL21 (DE3) competent *E. coli* cells. Cells containing the plasmid were grown overnight at 37°C from bacterial stocks on LB agar plates containing 50 µg ml^{-1} kanamycin. A single colony was inoculated into a 250 ml flask containing 50 ml LB with 50 µg ml^{-1} kanamycin and then shaken overnight at 37°C and 150 rev min^{-1}. 15 ml of the overnight culture was used to inoculate two 2 l flasks of 500 ml LB with 50 µg ml^{-1} kanamycin. The inoculated culture was incubated at 37°C with shaking at 225 rev min^{-1} for approximately 2 h to an OD_{600} of between 0.6 and 0.8. Protein expression was induced using 0.1 m*M* IPTG with incubation for at least 8 h at 20°C and 150 rev min^{-1}. The culture was centrifuged at 4000 rev min^{-1} for 20 min and the pellet was stored at −80°C.

2.1.2. Recombinant SRPN18 purification. Recombinant SRPN18 purification was performed as described previously, with the following modifications (Zhang *et al.*, 2015). Cell pellets from expression were resuspended in 50 ml buffer *A* (50 m*M* NaCl, 20 m*M* Tris–HCl pH 8.0) supplemented with protease-inhibitor cocktail (Roche). Cells were lysed by sonication (Vibra Cell High Intensity Ultrasonic Processor 750 W model), and soluble and insoluble fractions were separated by centrifugation at 10 000*g* for 30 min at 4°C. Soluble portions were retained and purified by nickel-affinity, ion-exchange and size-exclusion chromatography using an ÄKTAxpress purification system (GE Healthcare) at 4°C. The clarified lysate was loaded onto a 5 ml HisTrap HP column (GE Healthcare) at 1 ml min^{-1}. Bound proteins were washed with 25 ml buffer *A*. Nonspecifically bound proteins were then eluted using a gradient of buffer *B* (500 m*M* imidazole, 50 m*M* NaCl, 20 m*M* Tris–HCl pH 8.0). Elution of SRPN18 was carried out with a linear gradient from 10 to 100% buffer *B* over eight column volumes, and all elution peaks were collected and analyzed by SDS–PAGE. SRPN18-containing fractions were pooled and loaded onto a 5 ml HiTrap Q HP anion-exchange column (GE Healthcare) equilibrated with buffer *A*. Elution was carried out with a linear gradient from 0 to 100% buffer *C* (500 m*M* NaCl, 20 m*M* Tris pH 8.0) over 20 column volumes, and the purity of SRPN18 was analyzed by SDS–PAGE. SRPN18-containing fractions were pooled again and concentrated to 1.0 ml in a Vivaspin 20 10 kDa molecular-weight cutoff concentrator (GE Healthcare). The concentrated protein was loaded onto a Superdex 75 10 300 GL size-exclusion column (GE Healthcare) and eluted in buffer *D* (400 m*M* NaCl, 20 m*M* Tris pH 8.0) at 0.2 ml min^{-1}. Protein fractions were analyzed by SDS–PAGE and protein concentrations were determined by the Bradford assay using Coomassie Plus Protein Assay Reagent (Pierce) and bovine serum albumin as a standard (Sigma). SRPN18 fractions were pooled and concentrated for crystallization screening to 12.8 mg ml^{-1} in buffer *D via* a Vivaspin 20 10 kDa molecular weight cutoff concentrator (GE Healthcare).

Table 2
Crystallization.

Method	Vapor diffusion, sitting drop
Plate type	Sitting drop
Temperature (K)	293
Protein concentration	12.8
Buffer composition of protein solution	400 m*M* NaCl, 20 m*M* Tris pH 8.0
Composition of reservoir solution	25%(*w*/*v*) PEG 3350, 100 m*M* bis-tris, 200 m*M* NaCl, 20% PEG 400
Volume and ratio of drop	1 µl (1:1)
Volume of reservoir (µl)	75

2.2. Crystallization

Crystallization screening was conducted in high-throughput Compact 300 (Rigaku Reagents) sitting-drop vapor-diffusion plates at 20°C using 0.5 µl protein solution and 0.5 µl crystallization solution equilibrated against 100 µl of the latter (Table 2). Prismatic crystals were obtained in 3–4 d from Index HT screen (Hampton Research) condition F11 [25%(*w*/*v*) PEG 3350, 100 m*M* bis-tris pH 6.5, 200 m*M* NaCl]. Crystals were transferred into a solution consisting of crystallization

Table 3
Crystallographic data for SRPN18 refined to 1.45 Å resolution.

Values in parentheses are for the highest resolution shell.

Data collection	
Unit-cell parameters (Å)	a = 40.42, b = 87.49, c = 194.79
Space group	$P2_12_12_1$
Resolution (Å)	48.70–1.45 (1.47–1.45)
Wavelength (Å)	1.0000
Temperature (K)	100
Observed reflections	808528
Unique reflections	122919
$\langle I/\sigma(I)\rangle$	20.1 (2.5)
Completeness (%)	99.6 (98.9)
Multiplicity	6.6 (6.7)
R_{merge}† (%)	4.3 (84.1)
R_{meas}‡ (%)	4.7 (90.3)
$R_{p.i.m.}$‡ (%)	1.8 (34.6)
$CC_{1/2}$§	0.999 (0.746)
Refinement	
Resolution range (Å)	36.69–1.45
Reflections (working/test)	116670/6160
R/R_{free}¶ (%)	16.5/18.5
No. of atoms (protein/water)	5773/537
Model quality	
R.m.s. deviations	
Bond lengths (Å)	0.008
Bond angles (°)	0.974
Average B factors (Å^2)	
All atoms	25.0
Protein	24.3
Water	32.0
Coordinate error (maximum likelihood) (Å)	0.14
Ramachandran plot	
Most favored (%)	98.0
Additionally allowed (%)	2.0

† $R_{merge} = \sum_{hkl}\sum_i |I_i(hkl) - \langle I(hkl)\rangle| / \sum_{hkl}\sum_i I_i(hkl)$, where $I_i(hkl)$ is the intensity measured for the ith reflection and $\langle I(hkl)\rangle$ is the average intensity of all reflections with indices hkl. ‡ R_{meas} is the redundancy-independent (multiplicity-weighted) R_{merge} (Evans, 2006, 2011). $R_{p.i.m.}$ is the precision-indicating (multiplicity-weighted) R_{merge} (Diederichs & Karplus, 1997; Weiss, 2001). § $CC_{1/2}$ is the correlation coefficient of the mean intensities between two random half-sets of data (Karplus & Diederichs, 2012; Evans, 2012). ¶ $R = \sum_{hkl} ||F_{obs}| - |F_{calc}|| / \sum_{hkl} |F_{obs}|$; R_{free} is calculated in an identical manner using a randomly selected 5% of reflections that were not included in the refinement.

solution supplemented with 5% PEG 400 and equilibrated for 1 min. The crystals were then transferred into solutions containing increasing concentrations of PEG 400 from 5% to 25%(*w*/*v*) PEG 3350, 100 m*M* bis-tris pH 6.5, 200 m*M* NaCl, 20% PEG 400 before cooling and storing them in liquid nitrogen.

2.3. Data collection and processing

Initial X-ray diffraction data were collected at 93 K in the University of Kansas Protein Structure Laboratory using a Rigaku RU-H3R rotating-anode generator (Cu $K\alpha$) equipped with Osmic Blue focusing mirrors and a Rigaku R-AXIS IV^{++} image-plate detector. Higher resolution data were collected at the Advanced Photon Source beamline 17-ID using a Dectris PILATUS 6M pixel-array detector.

2.4. Structure solution and refinement

Intensities were integrated using *XDS* (Kabsch, 2010*a*,*b*) and the Laue class check and data scaling were performed with *AIMLESS* (Evans, 2011). The highest probability Laue class was *mmm* and space group $P2_12_12_1$. The Matthews coefficient (V_M; Matthews, 1968) and solvent content were estimated to be V_M = 4.0 Å^3 Da^{-1} with 69.2% solvent content and V_M = 2.0 Å^3 Da^{-1} with 38.5% solvent content for one and two molecules in the asymmetric unit, respectively. A homology model for molecular replacement was created with *CHAINSAW* (Stein, 2008) using the previously determined SRPN2 structure (PDB entry 3pzf), the amino-acid sequence of which is 37.9% similar to that of SRPN18 (An, Lovell *et al.*, 2011). Molecular-replacement searches for two molecules in the asymmetric unit were conducted using in-house diffraction data with *Phaser* (McCoy *et al.*, 2007) *via* the *PHENIX* (Adams *et al.*, 2010) interface in all possible space groups with point symmetry 222. The top solution was found in space

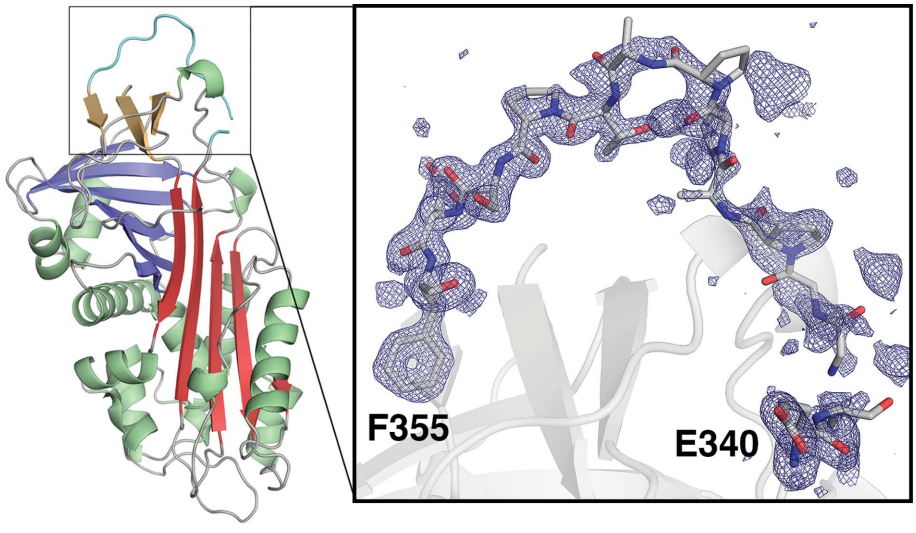

Figure 1
Crystal structure of SRPN18 including the reactive-center loop (RCL). (*a*) Ribbon diagram of the SRPN18 crystal structure determined to a resolution of 1.45 Å. β-Sheet A, red; β-sheet B, blue; β-sheet C, yellow; α-helices, green; RCL, cyan. (*b*) $F_o - F_c$ OMIT electron-density map (3σ) of the SRPN18 RCL (residues Glu340–Phe355). Map clipping is expanded to 5 Å from the RCL atoms.

Table 4
Serpin structures used for comparative structural analysis of the RCL with accessible surface area (ASA).

Serpin	Protease complex	Species	PDB code	Function	RCL residues	ASA (Å^2)	Reference
SRPN18		*Anopheles gambiae*	5c98		16	1095†	This work
Serpin 18		*Bombyx mori*	4r9i	Cysteine protease inhibitor, silk production	17	1273	Guo *et al.* (2015)
Ovalbumin		*Gallus gallus*	1ova	Non-inhibitory, storage protein	22	1318	Stein *et al.* (1991)
Hsp47		*Canis lupus familiaris*	3zha	Non-inhibitory, collagen chaperone	19	1473	Widmer *et al.* (2012)
Maspin		*Homo sapiens*	1xqg	Non-inhibitory, tumor suppression	20	1522	Al-Ayyoubi *et al.* (2004)
HCII		*Homo sapiens*	1jmj	Inhibitory, anti-coagulation	22	1524	Baglin *et al.* (2002)
ZPI	Protein Z	*Homo sapiens*	3h5c	Inhibitory, anti-coagulation	22	1663	Huang *et al.* (2010)
β-AT		*Homo sapiens*	1e04	Inhibitory, anti-coagulation	25	1714	McCoy *et al.* (2003)
Tengpin		*Thermoanaerobacter tengcongensis*	2pee	Inhibitory, unknown	24	1732	Zhang *et al.* (2007)
α-AT		*Homo sapiens*	1e03	Inhibitory, anti-coagulation	24	1800	McCoy *et al.* (2003)
PAI-1		*Homo sapiens*	1b3k	Inhibitory, anti-coagulation	21	1870	Sharp *et al.* (1999)
PN1	Thrombin	*Homo sapiens*	4dy7	Inhibitory, anti-coagulation	22	1883	Li & Huntington (2012)
SCCA1		*Homo sapiens*	2zv6	Inhibitory, anti-apoptotic	24	1983	Zheng *et al.* (2009)
PCI		*Homo sapiens*	2ol2	Inhibitory, anti-coagulation	24	2024	Li *et al.* (2007)
Alaserpin	Trypsin	*Manduca sexta*	1k9o	Inhibitory, development	24	2026	Ye *et al.* (2001)
MENT		*Gallus gallus*	2dut	Non-inhibitory, chromatin condensation	25	2039†	McGowan *et al.* (2006)
ACH		*Mus musculus*	1yxa	Inhibitory, anti-inflammation	25	2040	Horvath *et al.* (2005)
A1AT		*Homo sapiens*	1hp7	Inhibitory, anti-inflammation	22	2113	Kim *et al.* (2001)
PAI-1		*Danio rerio*	4dte	Inhibitory, anti-coagulation	22	2124	Bager *et al.* (2013)
Serpin 1K		*Manduca sexta*	1sek	Inhibitory, immunity	23	2281	Li *et al.* (1999)
α-AT	Factor IXa	*Homo sapiens*	3kcg	Inhibitory, anti-coagulation	24	2337	Johnson *et al.* (2010)
At-Serpin1		*Arabidopsis thaliana*	3le2	Inhibitory, anti-apoptotic	25	2357	Lampl *et al.* (2010)

† To determine the accessible surface area of the entire RCL in SRPN18 and MENT, unresolved residues (SRPN18, Gly342–Ser343; MENT, Ile375–Asn376) were modeled into the structure before calculation using *Coot* (Emsley *et al.*, 2010).

group $P2_12_12_1$ and consisted of a noncrystallographic dimer related by the spherical polar coordinates $\omega = 91.057^\circ$, $\varphi = -177.973^\circ$, $\chi = 176.861^\circ$ with the NCS axis is nearly parallel to the crystallographic *a* axis. Following initial refinement with *PHENIX*, the *R* factors converged at $R = 40\%$ and $R_{\rm free} = 44\%$. The model was improved using automated model building with *ARP*/*wARP* (Langer *et al.*, 2008) and the final model, refined against the synchrotron diffraction data, was obtained by iterative rounds of refinement and manual model building with *PHENIX* and *Coot* (Emsley *et al.*, 2010), respectively. Structure validation was conducted with *MolProbity* (Chen *et al.*, 2010). TLS refinement (Painter & Merritt, 2006; Winn *et al.*, 2001) was incorporated into the later stages of refinement to model anisotropic atomic displacement parameters. Residues Ser343–Ser353 of chain *A* and Ser341–Gly344 of chain *B*, which are part of the RCL, were disordered and could not be modeled. Disordered side-chain atoms were truncated to the point where electron density could be observed. Figures were prepared using *PyMOL* (Schrödinger). Solvent-accessible solvent area was determined using *AREAIMOL* (Lee & Richards, 1971; Saff & Kuijlaars, 1997) from the *CCP*4 program suite (Winn *et al.*, 2011). Relevant crystallographic data are provided in Table 3. Coordinates and structure factors were deposited in the Worldwide Protein Data Bank with accession code 5c98.

3. Results and discussion

3.1. Overall SRPN18 structure

We determined the crystal structure of *A. gambiae* SRPN18 (residues 23–391) to a resolution of 1.45 Å (Table 3). SRPN18 contains a conserved serpin fold with three β-sheets (A, B and C) surrounded by 13 α-helices (Fig. 1*a*). An analysis of the SRPN18 structure against the *DALI* database revealed a high degree of homology to a wide range of serpins owing to the conservation of the serpin fold, with a root-mean-square deviation (r.m.s.d.) between C^α atoms of SRPN18 and its closest structural homologs of approximately 2.3 Å (Supplementary Table S1).

SRPN18 crystallized as an NCS dimer with two molecules in the asymmetric unit (Supplementary Fig. S1). The two molecules are identical, with the exception of the observable electron density for the RCL (Glu340–Pro362). In chain *A* residues Gly344–Pro352 were disordered and could not be modeled, as is commonly found in serpin structures. However, the RCL of SRPN18 chain *B* was resolved completely, with the exception of two residues, Gly342 and Ser343 (Fig. 1*b*). The SRPN18 RCL in chain *B* forms a continuous loop and is located directly above β-sheet C. The RCL interacts directly with β-sheet C *via* multiple hydrogen bonds, which are also present between residues within the RCL itself.

3.2. Comparative structural analysis of the SRPN18 RCL

The RCL is integral to the canonical inhibitory activity of serpins. Therefore, the resolution of the SRPN18 RCL in chain *B* permitted investigation into the architecture of the RCL in order to gain insight into its potential role in SRPN18 inactivity. We performed a comparative structural analysis of the RCL of chain *B* in the SRPN18 structure and the RCLs of previously published serpin structures. This comparative analysis was performed with 21 serpin structures, all of which contain an RCL that is completely, or nearly completely, resolved (Table 4). The structures represent 17 distinct serpins: 13 are inhibitory against serine proteinases [protein

Z-dependent protease inhibitory protein (ZPI), heparin cofactor II (HCII), protease nexin-1 (PN1), plasminogen activator inhibitor-1 (PAI-1), 1-antitrypsin (A1AT), antithrombin (AT), AtSerpin1, alaserpin, antichymotrypsin (ACH), tengpin, squamous cell carcinoma antigen 1 (SCCA1), serpin 1K and protein C inhibitor (PCI)], one is inhibitory against cysteine proteinases (*Bombyx mori* serpin 18) and four are non-inhibitory [ovalbumin, heat-shock protein 47 (Hsp47), maspin and myeloid and erythroid nuclear termination stage-specific antigen (MENT)]. These structures provide a diverse and comprehensive basis to analyze the functional implications of the SRPN18 RCL structure.

The most conspicuous feature of the SRPN18 RCL is its short length compared with those of other serpins, spanning a total of 16 residues (Table 4). RCL length is a crucial factor for canonical serpin inhibition, as a sufficient RCL length is required for full insertion into β-sheet A (Huntington, 2011). The next shortest RCLs in our analysis belong to the cysteine proteinase inhibitor *B. mori* serpin 18 (which uses a distinct inhibitory mechanism) and the non-inhibitory Hsp47, which

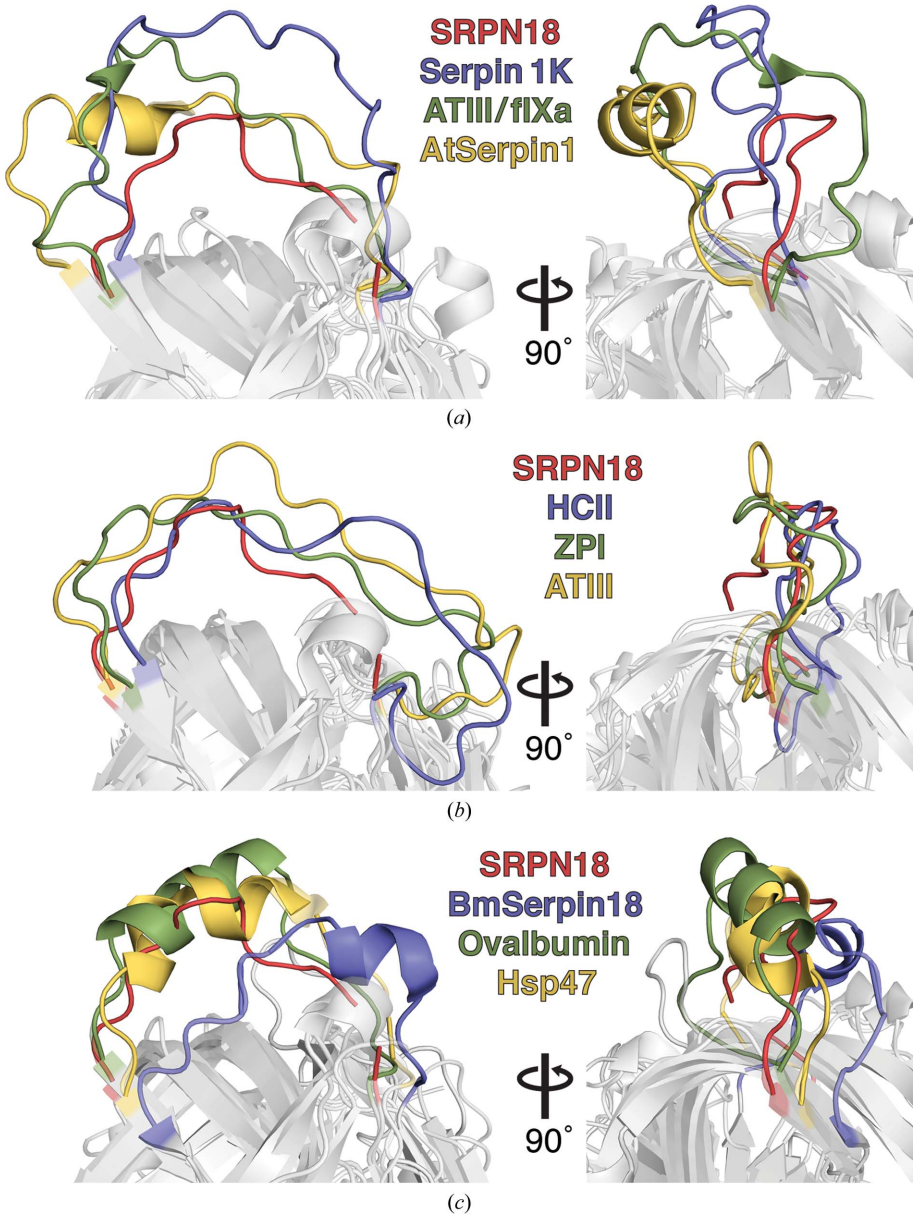

Figure 2
Structural alignment of the SRPN18 RCL with those of other serpins. The panel on the right is rotated 90° around the *y* axis. (*a*) Structural alignment of the SRPN18 RCL (red) with inhibitory serpins whose RCLs contain high accessible surface areas. Serpin 1K, PDB entry 1sek, blue (Li *et al.*, 1999); AT (in complex with factor IXa; ATIII/fIXa), PDB entry 3kcg, green (Johnson *et al.*, 2010); AtSerpin1, PDB entry 3le2, orange (Lampl *et al.*, 2010). (*b*) Structural alignment of the SRPN18 RCL (red) with inhibitory serpins whose RCLs contain low accessible surface areas. HCII, PDB entry 1jmj, blue (Baglin *et al.*, 2002); ZPI, PDB entry 3h5c, green (Huang *et al.*, 2010); AT, PDB entry 1e04, orange (McCoy *et al.*, 2003). (*c*) Structural alignment of the SRPN18 RCL with non-inhibitory or cysteine proteinase inhibitory (*B. mori* serpin 18; BmSerpin18) serpins with low accessibility scores. *B. mori* serpin 18, PDB entry 4r9i, blue (Guo *et al.*, 2015); ovalbumin, PDB entry 1ova, green (Stein *et al.*, 1991); Hsp47, PDB entry 3zha, orange (Widmer *et al.*, 2012).

contain 17 and 19 residues, respectively. The shortest RCL of an inhibitory serpin against serine proteinases is that of PAI-1, containing 21 residues. Among the inhibitory serpins in our analysis, the RCL length averages 23 residues and ranges from 21 to 25. The structures of AT, ZPI, PCI and PAI-1 have been determined in their cleaved state, with the RCL inserted into β-sheet A, and reveal a necessity for 16 RCL residues prior to the P1–P1′ scissile bond for full insertion (Schreuder *et al.*, 1994; Huang *et al.*, 2010; Li & Huntington, 2008; Jensen & Gettins, 2008). Thus, cleavage at even the most C-terminal residue in the SRPN18 RCL would result in an RCL segment that is too short for complete insertion, providing credence to previous assertions that it is non-inhibitory.

The length of the RCL also has implications for the accessibility of the RCL to the target protease (Johnson *et al.*, 2010; Jin *et al.*, 1997; Baglin *et al.*, 2002). In general, increased accessibility correlates with increased inhibition to the extent that RCL flexibility may be controlled allosterically to regulate the level of serpin activity. To determine the level of constriction of the SRPN18 RCL, accessible surface area (ASA) was quantified in all of the serpins included in our comparative analyses (Table 4). Indeed, the RCL of SRPN18

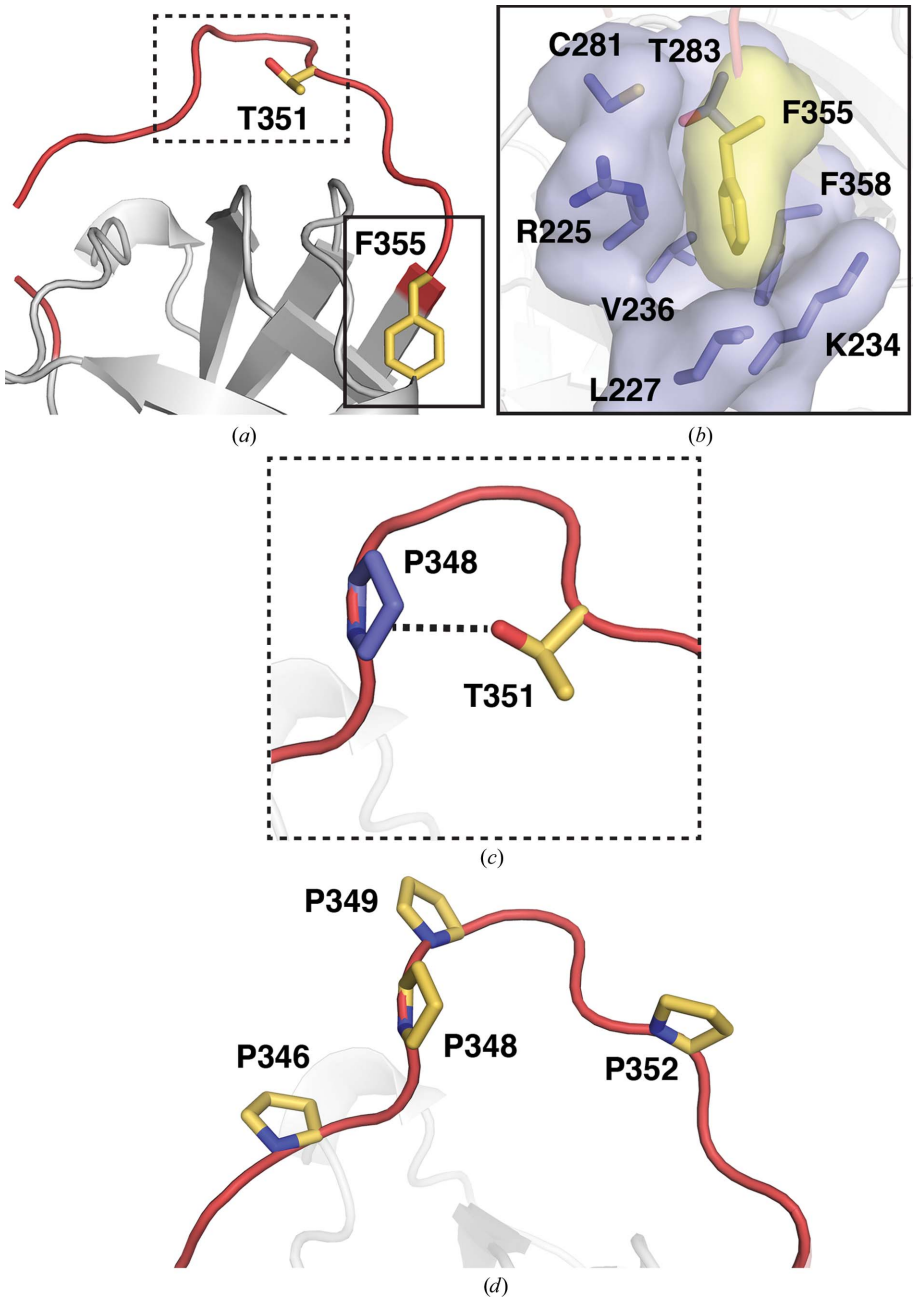

Figure 3
Features of the SRPN18 RCL that are not conducive towards inhibition. (*a*) The SRPN18 RCL (red) showing the side chains of Phe355 and Thr351 (yellow). (*b*) The area highlighted with a solid box in (*a*) showing Phe355 (yellow) buried within a pocket formed by residues found within β-sheet C (blue). (*c*) The area highlighted with a dotted box in (*a*) showing Thr351, which forms interactions with Pro348 (blue). (*d*) Location of the four proline residues in the SRPN18 RCL.

is extremely constricted in comparison to other serpins, with an ASA of 1095 Å^2, which was the lowest of any of the serpin structures in our analysis. The next lowest ASA was found for the cysteine proteinase inhibitor *B. mori* serpin 18 (1273 Å^2). Structural alignment of SRPN18 and inhibitory serpins with high ASAs [serpin 1K, 2281 Å^2; AT (in complex with factor IXa), 2337 Å^2; AtSerpin1, 2357 Å^2] highlights the level of constriction and the overall lack of flexibility inherent to the SRPN18 RCL (Fig. 2*a*). Inhibitory serpins that contain lower ASAs, closer to that of SRPN18 (HCII, 1524 Å^2; ZPI, 1663 Å^2; AT, 1714 Å^2), are found in structures containing partial RCL hinge-loop insertions, which are expelled to increase the accessibility of the RCL as a mechanism of allosteric regulation (Fig. 2*b*). The RCLs that most closely resemble SRPN18 are either cysteine proteinase inhibitors or non-inhibitory serpins (*B. mori* serpin 18; ovalbumin, 1318 Å^2; Hsp47, 1473 Å^2; Fig. 2*c*). It is interesting to note that all three of these RCLs contain α-helices and therefore do not directly resemble SRPN18. Together, these data suggest that the SRPN18 RCL is unprecedented with respect to its constriction and is likely to represent a minimum length that can be accommodated within the serpin fold.

In addition to the constrained overall accessibility of the SRPN18 RCL, the structure reveals the absence of an accessible P1 residue that can function as a bait for proteolytic attack. Previous studies tenuously predicted the most likely P1 residue for SRPN18 to be Phe355 based on sequence alignment (Gulley *et al.*, 2013; Suwanchaichinda & Kanost, 2009). However, the SRPN18 structure indicated that Phe355 is located at the C-terminus of the RCL and is buried within a pocket composed of Arg225, Leu227, Lys234, Val236, Phe358, Cys281 and Thr283 (Figs. 3*a* and 3*b*). Thus, Phe355 is not exposed to the solvent and is therefore inaccessible to a target protease. P1 residues in other serpins are invariably located towards the most solvent-exposed apex of the RCL and are commonly situated slightly towards the C-terminus as opposed to the hinge region (Huntington, 2011). In SRPN18 this region is occupied by Thr351, making it a potential candidate for a P1 residue (Fig. 3*a*). However, the structure revealed that Thr351 is directed away from the surface and that the hydroxyl group forms a hydrogen bond to Pro348 (Fig. 3*c*). As such, it appears to be incapable of acting as an effective P1 residue despite its position within the RCL. Thus, SRPN18 seems to lack a suitable P1 residue, which is critical for initiating the inhibitory mechanism. In addition, the SRPN18 RCL contains four proline residues (Pro346, Pro348, Pro349 and Pro352), three of which are found in the hinge region (Fig. 3*d*). Previous studies have shown that prolines located N-terminal to the P2 residue result in a breakdown of inhibitory function (Hopkins *et al.*, 1993; Hopkins & Stone, 1995; Gettins, 2002). This is because prolines disrupt β-strands, resulting in an inability of the RCL to insert completely into β-sheet A. Not surprisingly, proline residues prior to the P2 position in the RCL are almost exclusively found amongst non-inhibitory serpins, including Hsp47, maspin, thyroxine-binding globulin (TBG), corticosteroid-binding globulin (CBG) and pigment epithelium-derived factor (PEDF). In addition, the four prolines found in the SRPN18 RCL represent the extreme end of the spectrum. Analysis of 347 serpin primary sequences revealed only one instance (*Mesocricetus auratus* CBG, UniProtKB Q60543.1) of another serpin with four prolines in the RCL prior to the P2 residue, and only three instances (*Mus musculus* CBG, Q06770.1; *M. musculus* PEDF, P97298.2; *Homo sapiens* PEDF, P36955.4) of three prolines in this region of the RCL.

Overall, the SRPN18 RCL sequence and structure reveal several features associated with serpins that do not function *via* the canonical serine proteinase inhibitory mechanism: (i) minimal length, (ii) a constricted conformation, (iii) the absence of a suitable P1 residue and (iv) a large number of proline residues. Nevertheless, the expression pattern of SRPN18 and its maintenance through the evolutionary history of *A. gambiae* suggest that it serves a specific function (Gulley *et al.*, 2013; Suwanchaichinda & Kanost, 2009). An ortholog of SRPN18 in *Culex quinquefasciatus* (Bartholomay *et al.*, 2010), which contains a short RCL length and RCL prolines, suggests that SRPN18 was present in the common ancestor of both anopheline and culicine mosquitoes and has been maintained by evolution for at least 160 million years. Orthologs of SRPN18 are found in automatically annotated gene sets of the 16 additional recently sequenced anopheline genomes (Neafsey *et al.*, 2015). Their future refinement will provide additional information of possible conservation of key functional elements. Additional investigations will be necessary to determine the precise role of SRPN18 in *A. gambiae* and to determine how its unique structure operates to fulfill its role in the organism.

Acknowledgements

We thank Dr Fei Philip Gao for help with the SRPN18 purification. Use of the IMCA-CAT beamline 17-ID at the Advanced Photon Source was supported by the companies of the Industrial Macromolecular Crystallography Association through a contract with Hauptman–Woodward Medical Research Institute. Use of the Advanced Photon Source was supported by the US Department of Energy, Office of Science, Office of Basic Energy Sciences under Contract No. DE-AC02-06CH11357. The research reported in this publication was supported by the Institute of Allergy and Infectious Diseases of the National Institutes of Health under award No. R01AI095842 (to KM). The use of the KU COBRE Protein Structure Laboratory was supported by NIH Grant No. P30 GM110761 from the National Institute of General Medical Sciences. Its contents are solely the responsibility of the authors and do not necessarily represent the official views of the Center of Biomedical Research Excellence in Protein Structure and Function or the National Institutes of Health. This is contribution 17-119-J from the Kansas Agricultural Experiment Station.

References

Abraham, E. G., Pinto, S. B., Ghosh, A., Vanlandingham, D. L., Budd, A., Higgs, S., Kafatos, F. C., Jacobs-Lorena, M. & Michel, K. (2005). *Proc. Natl Acad. Sci. USA*, **102**, 16327–16332.

Adams, P. D. *et al.* (2010). *Acta Cryst.* D**66**, 213–221.
Al-Ayyoubi, M., Gettins, P. G. W. & Volz, K. (2004). *J. Biol. Chem.* **279**, 55540–55544.
Al-Horani, R. A. (2014). *Cardiovasc. Hematol. Agents Med. Chem.* **12**, 91–125.
An, C., Budd, A., Kanost, M. R. & Michel, K. (2011). *Cell. Mol. Life Sci.* **68**, 1929–1939.
An, C., Lovell, S., Kanost, M. R., Battaile, K. P. & Michel, K. (2011). *Proteins*, **79**, 1999–2003.
Annand, R. R., Dahlen, J. R., Sprecher, C. A., De Dreu, P., Foster, D. C., Mankovich, J. A., Talanian, R. V., Kisiel, W. & Giegel, D. A. (1999). *Biochem. J.* **342**, 655–665.
Ashton-Rickardt, P. G. (2013). *Immunol. Lett.* **152**, 65–76.
Bager, R., Johansen, J. S., Jensen, J. K., Stensballe, A., Jendroszek, A., Buxbom, L., Sørensen, H. P. & Andreasen, P. A. (2013). *J. Mol. Biol.* **425**, 2867–2877.
Baglin, T. P., Carrell, R. W., Church, F. C., Esmon, C. T. & Huntington, J. A. (2002). *Proc. Natl Acad. Sci. USA*, **99**, 11079–11084.
Barillas-Mury, C. (2007). *Trends Parasitol.* **23**, 297–299.
Bartholomay, L. C. *et al.* (2010). *Science*, **330**, 88–90.
Chaillan-Huntington, C. E., Gettins, P. G. W., Huntington, J. A. & Patston, P. A. (1997). *Biochemistry*, **36**, 9562–9570.
Chen, V. B., Arendall, W. B., Headd, J. J., Keedy, D. A., Immormino, R. M., Kapral, G. J., Murray, L. W., Richardson, J. S. & Richardson, D. C. (2010). *Acta Cryst.* D**66**, 12–21.
Christophides, G. K. *et al.* (2002). *Science*, **298**, 159–165.
Christophides, G. K., Vlachou, D. & Kafatos, F. C. (2004). *Immunol. Rev.* **198**, 127–148.
Danielli, A., Kafotos, F. C. & Loukeris, T. G. (2003). *J. Biol. Chem.* **278**, 4184–4193.
Declerck, P. J. & Gils, A. (2013). *Semin. Thromb. Hemost.* **39**, 356–364.
Diederichs, K. & Karplus, P. A. (1997). *Nature Struct. Mol. Biol.* **4**, 269–275.
Dunstone, M. A. & Whisstock, J. C. (2011). *Methods Enzymol.* **501**, 63–87.
Emsley, P., Lohkamp, B., Scott, W. G. & Cowtan, K. (2010). *Acta Cryst.* D**66**, 486–501.
Evans, P. (2006). *Acta Cryst.* D**62**, 72–82.
Evans, P. (2011). *Acta Cryst.* D**67**, 282–292.
Evans, P. (2012). *Science*, **336**, 986–987.
Fish, W. W. & Bjork, I. (1979). *Eur. J. Biochem.* **101**, 31–38.
Francis, S. E., Ersoy, R. A., Ahn, J.-W., Atwell, B. J. & Roberts, T. H. (2012). *BMC Genomics*, **13**, 449.
Gatto, M., Iaccarino, L., Ghirardello, A., Bassi, N., Pontisso, P., Punzi, L., Shoenfeld, Y. & Doria, A. (2013). *Clin. Rev. Allerg. Immunol.* **45**, 267–280.
Gettins, P. G. W. (2002). *Chem. Rev.* **102**, 4751–4804.
Gubb, D., Sanz-Parra, A., Barcena, L., Troxler, L. & Fullaondo, A. (2010). *Biochimie*, **92**, 1749–1759.
Gulley, M. M., Zhang, X. & Michel, K. (2013). *J. Insect Physiol.* **59**, 138–147.
Guo, P.-C., Dong, Z., Zhao, P., Zhang, Y., He, H., Tan, X., Zhang, W. & Xia, Q. (2015). *Sci. Rep.* **5**, 11863.
Hashimoto, C., Kim, D. R., Weiss, L. A., Miller, J. W. & Morisato, D. (2003). *Dev. Cell*, **5**, 945–950.
Hood, D. B., Huntington, J. A. & Gettins, P. G. W. (1994). *Biochemistry*, **33**, 8538–8547.
Hopkins, P. C., Carrell, R. W. & Stone, S. R. (1993). *Biochemistry*, **32**, 7650–7657.
Hopkins, P. C. & Stone, S. R. (1995). *Biochemistry*, **34**, 15872–15879.
Horvath, A. J., Irving, J. A., Rossjohn, J., Law, R. H., Bottomley, S. P., Quinsey, N. S., Pike, R. N., Coughlin, P. B. & Whisstock, J. C. (2005). *J. Biol. Chem.* **280**, 43168–43178.
Huang, X., Dementiev, A., Olson, S. T. & Gettins, P. G. W. (2010). *J. Biol. Chem.* **285**, 20399–20409.
Huasong, G., Zongmei, D., Jianfeng, H., Xiaojun, Q., Jun, G., Sun, G., Donglin, W. & Jianhong, Z. (2015). *Brain Res.* **1600**, 59–69.
Hughes, G. L., Ren, X., Ramirez, J. L., Sakamoto, J. M., Bailey, J. A., Jedlicka, A. E. & Rasgon, J. L. (2011). *PLoS Pathog.* **7**, e1001296.
Huntington, J. A. (2006). *Trends Biochem. Sci.* **31**, 427–435.
Huntington, J. A. (2011). *J. Thromb. Haemost.* **9**, 26–34.
Huntington, J. A. (2013). *J. Thromb. Haemost.* **11**, 254–264.
Huntington, J. A., Fan, B., Karlsson, K. E., Deinum, J., Lawrence, D. A. & Gettins, P. G. W. (1997). *Biochemistry*, **36**, 5432–5440.
Huntington, J. A., McCoy, A., Belzar, K. J., Pei, X. Y., Gettins, P. G. W. & Carrell, R. W. (2000). *J. Biol. Chem.* **275**, 15377–15383.
Huntington, J. A., Read, R. J. & Carrell, R. W. (2000). *Nature (London)*, **407**, 923–926.
Irving, J. A., Pike, R. N., Lesk, A. M. & Whisstock, J. C. (2000). *Genome Res.* **10**, 1845–1864.
Jensen, J. K. & Gettins, P. G. W. (2008). *Protein Sci.* **17**, 1844–1849.
Jin, L., Abrahams, J. P., Skinner, R., Petitou, M., Pike, R. N. & Carrell, R. W. (1997). *Proc. Natl Acad. Sci. USA*, **94**, 14683–14688.
Johnson, D. J., Langdown, J. & Huntington, J. A. (2010). *Proc. Natl Acad. Sci. USA*, **107**, 645–650.
Kabsch, W. (2010*a*). *Acta Cryst.* D**66**, 125–132.
Kabsch, W. (2010*b*). *Acta Cryst.* D**66**, 133–144.
Kambris, Z., Blagborough, A. M., Pinto, S. B., Blagrove, M. S., Godfray, H. C., Sinden, R. E. & Sinkins, S. P. (2010). *PLoS Pathog.* **6**, e1001143.
Karplus, P. A. & Diederichs, K. (2012). *Science*, **336**, 1030–1033.
Kim, S.-J., Woo, J.-R., Seo, E. J., Yu, M.-H. & Ryu, S.-E. (2001). *J. Mol. Biol.* **306**, 109–119.
Klieber, M. A., Underhill, C., Hammond, G. L. & Muller, Y. A. (2007). *J. Biol. Chem.* **282**, 29594–29603.
Lampl, N., Budai-Hadrian, O., Davydov, O., Joss, T. V., Harrop, S. J., Curmi, P. M., Roberts, T. H. & Fluhr, R. (2010). *J. Biol. Chem.* **285**, 13550–13560.
Langer, G., Cohen, S. X., Lamzin, V. S. & Perrakis, A. (2008). *Nature Protoc.* **3**, 1171–1179.
Lee, B. & Richards, F. M. (1971). *J. Mol. Biol.* **55**, 379–400.
Li, J., Wang, Z., Canagarajah, B., Jiang, H., Kanost, M. & Goldsmith, E. J. (1999). *Structure*, **7**, 103–109.
Li, W., Adams, T. E., Kjellberg, M., Stenflo, J. & Huntington, J. A. (2007). *J. Biol. Chem.* **282**, 13759–13768.
Li, W. & Huntington, J. A. (2008). *J. Biol. Chem.* **283**, 36039–36045.
Li, W. & Huntington, J. A. (2012). *Blood*, **120**, 459–467.
Ligoxygakis, P., Roth, S. & Reichhart, J. M. (2003). *Curr. Biol.* **13**, 2097–2102.
Loebermann, H., Tokuoka, R., Deisenhofer, J. & Huber, R. (1984). *J. Mol. Biol.* **177**, 531–557.
Mahajan, N., Shi, H. Y., Lukas, T. J. & Zhang, M. (2013). *J. Biol. Chem.* **288**, 11611–11620.
Marinotti, O., Calvo, E., Nguyen, Q. K., Dissanayake, S., Ribeiro, J. M. & James, A. A. (2006). *Insect Mol. Biol.* **15**, 1–12.
Mast, A. E., Enghild, J. J. & Salvesen, G. (1992). *Biochemistry*, **31**, 2720–2728.
Matthews, B. W. (1968). *J. Mol. Biol.* **33**, 491–497.
McCarthy, B. J. & Worrall, D. M. (1997). *J. Mol. Biol.* **267**, 561–569.
McCoy, A. J., Grosse-Kunstleve, R. W., Adams, P. D., Winn, M. D., Storoni, L. C. & Read, R. J. (2007). *J. Appl. Cryst.* **40**, 658–674.
McCoy, A. J., Pei, X. Y., Skinner, R., Abrahams, J. P. & Carrell, R. W. (2003). *J. Mol. Biol.* **326**, 823–833.
McGowan, S., Buckle, A. M., Irving, J. A., Ong, P. C., Bashtannyk-Puhalovich, T. A., Kan, W.-T., Henderson, K. N., Bulynko, Y. A., Popova, E. Y., Smith, A. I., Bottomley, S. P., Rossjohn, J., Grigoryev, S. A., Pike, R. N. & Whisstock, J. C. (2006). *EMBO J.* **25**, 3144–3155.
Meekins, D. A., Kanost, M. R. & Michel, K. (2016). *Semin. Cell Dev. Biol.* https://doi.org/10.1016/j.semcdb.2016.09.001.
Michel, K., Budd, A., Pinto, S., Gibson, T. J. & Kafatos, F. C. (2005). *EMBO Rep.* **6**, 891–897.
Neafsey, D. E. *et al.* (2015). *Science*, **347**, 1258522.
Olson, S. T. & Gettins, P. G. W. (2011). *Prog. Mol. Biol. Transl. Sci.* **99**, 185–240.
Painter, J. & Merritt, E. A. (2006). *Acta Cryst.* D**62**, 439–450.

Rau, J. C., Beaulieu, L. M., Huntington, J. A. & Church, F. C. (2007). *J. Thromb. Haemost.* **5**, Suppl. 1, 102–115.
Ravenhill, L., Wagstaff, L., Edwards, D. R., Ellis, V. & Bass, R. (2010). *J. Biol. Chem.* **285**, 36285–36292.
Saff, E. B. & Kuijlaars, A. B. J. (1997). *Math. Intelligencer*, **19**, 5–11.
Schick, C., Bromme, D., Bartuski, A. J., Uemura, Y., Schechter, N. M. & Silverman, G. A. (1998). *Proc. Natl Acad. Sci. USA*, **95**, 13465–13470.
Schreuder, H. A., de Boer, B., Dijkema, R., Mulders, J., Theunissen, H. J. M., Grootenhuis, P. D. & Hol, W. G. J. (1994). *Nature Struct. Mol. Biol.* **1**, 48–54.
Sharp, A. M., Stein, P. E., Pannu, N. S., Carrell, R. W., Berkenpas, M. B., Ginsburg, D., Lawrence, D. A. & Read, R. J. (1999). *Structure*, **7**, 111–118.
Silverman, G. A., Whisstock, J. C., Bottomley, S. P., Huntington, J. A., Kaiserman, D., Luke, C. J., Pak, S. C., Reichhart, J. M. & Bird, P. I. (2010). *J. Biol. Chem.* **285**, 24299–24305.
Simonovic, M., Gettins, P. G. W. & Volz, K. (2001). *Proc. Natl Acad. Sci. USA*, **98**, 11131–11135.
Stein, N. (2008). *J. Appl. Cryst.* **41**, 641–643.
Stein, P. E., Leslie, A. G. W., Finch, J. T. & Carrell, R. W. (1991). *J. Mol. Biol.* **221**, 941–959.
Stein, P. E., Tewkesbury, D. A. & Carrell, R. W. (1989). *Biochem. J.* **262**, 103–107.
Stratikos, E. & Gettins, P. G. W. (1999). *Proc. Natl Acad. Sci. USA*, **96**, 4808–4813.
Suwanchaichinda, C. & Kanost, M. R. (2009). *Gene*, **442**, 47–54.
Weiss, M. S. (2001). *J. Appl. Cryst.* **34**, 130–135.
Whisstock, J. C. & Bottomley, S. P. (2006). *Curr. Opin. Struct. Biol.* **16**, 761–768.
Widmer, C., Gebauer, J. M., Brunstein, E., Rosenbaum, S., Zaucke, F., Drogemuller, C., Leeb, T. & Baumann, U. (2012). *Proc. Natl Acad. Sci. USA*, **109**, 13243–13247.
Winn, M. D. *et al.* (2011). *Acta Cryst.* D**67**, 235–242.
Winn, M. D., Isupov, M. N. & Murshudov, G. N. (2001). *Acta Cryst.* D**57**, 122–133.
Yamamoto, N., Kinoshita, T., Nohata, N., Yoshino, H., Itesako, T., Fujimura, L., Mitsuhashi, A., Usui, H., Enokida, H., Nakagawa, M., Shozu, M. & Seki, N. (2013). *Int. J. Oncol.* **43**, 1855–1863.
Ye, S., Cech, A. L., Belmares, R., Bergstrom, R. C., Tong, Y., Corey, D. R., Kanost, M. R. & Goldsmith, E. J. (2001). *Nature Struct. Biol.* **8**, 979–983.
Zhang, Q., Buckle, A. M., Law, R. H., Pearce, M. C., Cabrita, L. D., Lloyd, G. J., Irving, J. A., Smith, A. I., Ruzyla, K., Rossjohn, J., Bottomley, S. P. & Whisstock, J. C. (2007). *EMBO Rep.* **8**, 658–663.
Zhang, X., Meekins, D. A., An, C., Zolkiewski, M., Battaile, K. P., Kanost, M. R., Lovell, S. & Michel, K. (2015). *J. Biol. Chem.* **290**, 2946–2956.
Zheng, B., Matoba, Y., Kumagai, T., Katagiri, C., Hibino, T. & Sugiyama, M. (2009). *Biochem. Biophys. Res. Commun.* **380**, 143–147.
Zhou, Q., Snipas, S., Orth, K., Muzio, M., Dixit, V. M. & Salvesen, G. S. (1997). *J. Biol. Chem.* **272**, 7797–7800.
Zhou, A., Wei, Z., Read, R. J. & Carrell, R. W. (2006). *Proc. Natl Acad. Sci. USA*, **103**, 13321–13326.